Interfacial ferromagnetism and atomic structures in high-temperature grown Fe_3O_4/Pt/Fe_3O_4 epitaxial trilayers (EP)

T. Kikkawa (iD), M. Suzuki, R. Ramos (iD), M. H. Aguirre (iD), J. Okabayashi, K. Uchida (iD), I. Lucas, A. Anadón, D. Kikuchi, P. A. Algarabel (iD), L. Morellón (iD), M. R. Ibarra, and E. Saitoh

COLLECTIONS

(EP) This paper was selected as an Editor's Pick

View Online   Export Citation   CrossMark

ARTICLES YOU MAY BE INTERESTED IN

Introduction to antiferromagnetic magnons
Journal of Applied Physics **126**, 151101 (2019); https://doi.org/10.1063/1.5109132

Incomplete ionization in aluminum-doped 4H-silicon carbide
Journal of Applied Physics **126**, 145701 (2019); https://doi.org/10.1063/1.5120707

Interface-induced anomalous Nernst effect in Fe_3O_4/Pt-based heterostructures
Applied Physics Letters **114**, 113902 (2019); https://doi.org/10.1063/1.5063553

Interfacial ferromagnetism and atomic structures in high-temperature grown Fe₃O₄/Pt/Fe₃O₄ epitaxial trilayers (EP)

T. Kikkawa,[1,2,a)] (ID) M. Suzuki,[3] R. Ramos,[1] (ID) M. H. Aguirre,[4,5,6,7] (ID) J. Okabayashi,[8] K. Uchida,[2,9,10] (ID) I. Lucas,[4,5,7] A. Anadón,[4,5,11] D. Kikuchi,[1,2] P. A. Algarabel,[5,12] (ID) L. Morellón,[4,5,7] (ID) M. R. Ibarra,[4,5,6,7] and E. Saitoh[1,2,10,13,14]

AFFILIATIONS

[1]WPI Advanced Institute for Materials Research, Tohoku University, Sendai 980-8577, Japan
[2]Institute for Materials Research, Tohoku University, Sendai 980-8577, Japan
[3]Japan Synchrotron Radiation Research Institute (JASRI), Sayo, Hyogo 679-5198, Japan
[4]Instituto de Nanociencia de Aragón (INA), Universidad de Zaragoza, E-50018 Zaragoza, Spain
[5]Departamento de Física de la Materia Condensada, Universidad de Zaragoza, E-50009 Zaragoza, Spain
[6]Laboratorio de Microscopías Avanzadas, Universidad de Zaragoza, E-50018 Zaragoza, Spain
[7]Fundación Instituto de Nanociencia de Aragón (FINA), E-50018 Zaragoza, Spain
[8]Research Center for Spectrochemistry, The University of Tokyo, Bunkyo, Tokyo 113-0033, Japan
[9]National Institute for Materials Science, Tsukuba 305-0047, Japan
[10]Center for Spintronics Research Network, Tohoku University, Sendai 980-8577, Japan
[11]IMDEA Nanociencia, 28049 Madrid, Spain
[12]Instituto de Ciencia de Materiales de Aragón, Universidad de Zaragoza and Consejo Superior de Investigaciones Científicas, E-50009 Zaragoza, Spain
[13]Department of Applied Physics, The University of Tokyo, Tokyo 113-8656, Japan
[14]Advanced Science Research Center, Japan Atomic Energy Agency, Tokai 319-1195, Japan

[a)]**Electronic mail:** t.kikkawa@imr.tohoku.ac.jp

ABSTRACT

Induced Pt ferromagnetism in $Fe_3O_4/Pt/Fe_3O_4$ epitaxial trilayer films has been investigated by means of X-ray magnetic circular dichroism (XMCD) at the Pt $L_{3,2}$-edges at various temperatures from 300 K to 12 K, including the metal-insulator transition temperature of Fe_3O_4 ($T_V \sim 114$ K). At all the temperatures, we observed clear XMCD signals due to Pt ferromagnetism, the amplitude of which was determined to be $0.39\mu_B$ at 300 K and $0.52\mu_B$ at 12 K for the sample with the Pt thickness of $\sim$2 nm. Interestingly, these values are comparable to or even greater than those in Pt/$3d$-ferromagnetic-metal (Fe, Ni, Co, and $Ni_{81}Fe_{19}$) junction systems. The results can be interpreted in terms of a possible Fe interdiffusion into the Pt layer and also possible Fe-Pt alloying due to its high-temperature deposition.

I. INTRODUCTION

Multilayer systems comprising paramagnetic-metal and magnetic-oxide layers have widely been used for spin-current generation and detection.[1] Important examples include spin Seebeck effects (SSEs)[2,3] and spin Hall magnetoresistance (SMR).[4,5] SSE refers to the generation of a spin current from a heat current in a magnetic material. The spin current is converted into a measurable voltage via the inverse spin Hall effect (ISHE)[6,7] in an attached metal. SMR refers to the resistance modulation due to the simultaneous action of SHE and ISHE in a metal layer depending on the magnetization orientation in a magnetic layer. Both in SSE and SMR, Pt has often been used as a paramagnetic-metal layer due to its high SHE and ISHE efficiency,

while various garnet ferrites (e.g., $Y_3Fe_5O_{12}$[2-5,8] and $Gd_3Fe_5O_{12}$[9]) and spinel ferrites (e.g., $NiFe_2O_4$,[8,10] $CoFe_2O_4$,[11-13] $CoCr_2O_4$,[14] and Fe_3O_4[8,15-21]) have been used as a magnetic layer.

In parallel with SMR or SSE, magnetic proximity effects in Pt/magnetic-oxide systems have also been studied extensively. This is because, if the proximity-induced Pt ferromagnetism exists in these systems, the ISHE voltage induced by the spin-current phenomena may be contaminated by the anisotropic magnetoresistance or anomalous Nernst effect due to the magnetized Pt.[3,4,8,21-28] Hence, the separation of the spin-current contribution from magnetic-proximity-effect contribution is important in spintronics, and the detection of Pt ferromagnetism in the Pt/magnetic-oxide systems has attracted much attention.[29-38] Recent studies demonstrated that, in $Pt/Y_3Fe_5O_{12}$, $Pt/NiFe_2O_4$, $Pt/CoFe_2O_4$, and Pt/Fe_3O_4, the proximity-induced parasitic contribution is negligibly small in comparison with the spin-current contribution to SMR or SSE.[4,8,15,17,24-27,29,31-35,39]

To investigate the proximity-induced ferromagnetism, X-ray magnetic circular dichroism (XMCD)[40-42] and X-ray resonant magnetic reflectivity (XRMR)[43] techniques have been frequently used. Since the end of the 1990s, a number of XMCD and XRMR studies focusing on Pt/3d-ferromagnetic-metal (Fe, Ni, Co, and $Ni_{81}Fe_{19}$) junction systems have been reported and the Pt ferromagnetism in these systems has been established.[44-56] Recently, these techniques were applied for the Pt/magnetic-oxide systems: $Pt/Y_3Fe_5O_{12}$,[29-31,36] $Pt/NiFe_2O_4$,[32,33,37] $Pt/CoFe_2O_4$,[34,35,37] $Pt/MnFe_2O_4$,[37] and Pt/Fe_3O_4;[37] in contrast to the Pt/3d-ferromagnetic-metal systems, the proximity-induced Pt ferromagnetism in these Pt/magnetic-oxide systems was found to be undetectably small when the effect of Pt oxidization is negligible.[30,31] These results suggest that small magnetization of the magnetic oxides is disadvantageous to inducing proximity ferromagnetism in the adjacent Pt layer; $Y_3Fe_5O_{12}$, $NiFe_2O_4$, $CoFe_2O_4$, and Fe_3O_4 are insulators or highly-resistive conductors[57-59] and their volume magnetization is much smaller than that of the 3d-ferromagnetic-metals.[60]

In this paper, by means of XMCD at the Pt $L_{3,2}$-edges, we measured induced Pt ferromagnetism in $Fe_3O_4/Pt(t_{Pt} \sim 2$ and 5 nm)/Fe_3O_4 epitaxial trilayer samples at various temperatures ranging from $T = 300$ K to 12 K, including the metal-insulator transition temperature T_V of Fe_3O_4; above (below) $T_V \sim 114$ K, Fe_3O_4 is a resistive conductor (insulator). Thermal spin transport in Pt/Fe_3O_4 epitaxial multilayers has been investigated intensively[17-21,61] since some of the present authors successfully fabricated the high-quality epitaxial films.[17] However, a possible role of the proximity-induced Pt ferromagnetism remains to be clarified.[21] To investigate the Pt magnetic properties via XMCD, we prepared $Fe_3O_4/Pt/Fe_3O_4$ epitaxial films, where the Pt layers were sandwiched between Fe_3O_4 films and deposited with high-temperature sputtering to realize the epitaxial growth, as with the previous works.[17-21,61] We observed a remarkably large Pt ferromagnetic moment in the $Fe_3O_4/Pt/Fe_3O_4$ systems, which is comparable to or even greater than those in the conventional Pt/3d-ferromagnetic-metal junction systems. The XMCD signal monotonically increases with decreasing temperature from $T = 300$ K to 12 K, across $T_V \sim 114$ K of Fe_3O_4. The result is distinct from the recent XMCD study in a Pt(2 nm)/Fe_3O_4 film prepared at room

temperature,[37] which reports the undetectably small XMCD signals at the temperatures both above and below T_V.

This paper is organized as follows. In Sec. II, we show the sample preparation procedure and the details on the experimental setup for XMCD measurements. In Sec. III A, our samples are characterized in terms of X-ray diffraction (XRD), transmission electron spectroscopy, electrical conductivity, and magnetization. From Secs. III B–III E, we show the systematic experimental results on X-ray absorption spectra (XAS) and XMCD in our samples and also discuss them. Section IV is devoted to summarizing the present study.

II. SAMPLE PREPARATION AND EXPERIMENTAL SETUP

The $Fe_3O_4(46$ nm)/$Pt(\sim 2$ nm)/$Fe_3O_4(54$ nm) trilayer sample was grown on MgO (001) substrates by means of pulsed laser deposition (PLD) (for Fe_3O_4) and sputtering (for Pt) at a high temperature of $\sim 480\,°C$, which allows single-crystalline epitaxial growth.[17,18,62,63] All the growth processes were done in situ without breaking vacuum, because our PLD and sputtering systems share the same vacuum chamber. The base pressure was around 1×10^{-9} Torr. For the Fe_3O_4 growth, polycrystalline Fe_3O_4 target was ablated with a KrF excimer laser with 248 nm wavelength and 10 Hz repetition rate. The Fe_3O_4 deposition was done without introducing gas at the substrate temperature of $\sim 480\,°C$, which results in a chamber pressure of $\sim 1 \times 10^{-6}$ Torr. Without any posttreatments for the Fe_3O_4 and also without changing the temperature, the in situ Pt growth was carried out by DC magnetron sputtering with an Ar pressure of 0.5 mTorr. After forming the Pt layer, the top Fe_3O_4 layer was formed by PLD under the same condition as that for the first Fe_3O_4 layer on the MgO substrate. After the growth of the top Fe_3O_4 layer was completed, the substrate temperature was cooled down to room temperature at the rate of $10\,°C/min$. We note that in Ref. 63, some of the present authors reported the absence of other Fe phases apart from Fe_3O_4 in the Fe_3O_4 films, fabricated by the same procedure, by means of X-ray photoemission spectroscopy (XPS) on Fe 2p core level in Fe_3O_4 films, where the electronic state only in the near-surface region ($\lesssim 1$ nm from the surface[64]) is detected. To check the effect of Pt thickness on XMCD, we also fabricated a similar $Fe_3O_4/Pt/Fe_3O_4$ sample with the Pt thickness of $t_{Pt} \sim 5$ nm under the same condition. Besides, a $Pt(\sim 5$ nm)/$Fe_3O_4(40$ nm)/$Pt(\sim 2 - 3$ nm)/$Fe_3O_4(47$ nm) sample was prepared to investigate possible Fe contamination in the (top) Pt film formed on Fe_3O_4 via X-ray absorption spectra (XAS) and XMCD measurements at the Fe $L_{3,2}$-edges.

The XMCD experiments at the Pt $L_{3(2)}$-edge $[2p_{3/2(1/2)} \rightarrow 5d$ transition] were performed at the beamline BL39XU of SPring-8 synchrotron radiation facility using the fluorescence detection mode.[48] XAS were recorded with circularly-polarized X-rays while reversing their helicity at 1 Hz. The circularly-polarized X-rays with a high degree of polarization ($\geq 95\%$) were generated by using a diamond X-ray phase retarder. The Pt $L_{\alpha(\beta)}$ [for the Pt $L_{3(2)}$-edge] fluorescences were measured with a silicon drift detector. During the XMCD measurements, the $Fe_3O_4/Pt(t_{Pt} \sim 2$ and 5 nm)/$Fe_3O_4//MgO$ sample was placed in an electromagnet, where an external magnetic field, H, was applied to the sample at the angle of 5° with respect to the sample surface. Here, the H direction was parallel or antiparallel

to the direction of the angular momentum vector of the incident X-ray beam. The measurements of element-specific magnetization (ESM) curves were also carried out at the constant energy of $E = 11\,569$ eV (the XMCD peak position for the Pt L_3-edge) in the range of $|H| \leq 20$ kOe at $T = 300$ K and $|H| \leq 12$ kOe at $T = 12$ K.

III. RESULTS AND DISCUSSION

A. Sample characterization

1. X-ray diffraction

Figure 1 shows the X-ray diffraction (XRD) patterns of the $Fe_3O_4/Pt(\sim 2\,nm)/Fe_3O_4//MgO$ sample around the (002) Bragg peak from the MgO substrate. We observed the (004) reflection from the Fe_3O_4 layers as well as the (002) reflection from the Pt layer, which confirms the out-of-plane orientation of $Fe_3O_4[001]/Pt[001]/Fe_3O_4[001]//MgO[001]$. As shown in the inset to Fig. 1, the (004) reflection of Fe_3O_4 consists of two peaks with slightly different peak angles, 43.20° and 43.30°, marked with blue and red triangles, respectively. This result is due to the different underlayers for each Fe_3O_4 layer; the peak at the lower (higher) angle can be attributed to the diffraction from the Fe_3O_4 layer grown on the MgO substrate (grown on the Pt film), since the peak position at the lower one is in agreement with that of the (004) reflection from a Fe_3O_4 film grown on a MgO (001) substrate.[17] From the positions of the diffraction peaks, the out-of-plane lattice constants for the Fe_3O_4 layers grown on the MgO substrate and grown on the Pt film were, respectively, determined to be 8.370 Å and 8.352 Å. The Laue oscillations of the (004) reflection were observed for both the Fe_3O_4 layers, indicating high crystalline coherence of each Fe_3O_4 layer.

2. Transmission electron microscopy

To further investigate the structural quality of the $Fe_3O_4/Pt(\sim 2\,nm)/Fe_3O_4$ sample, we performed transmission
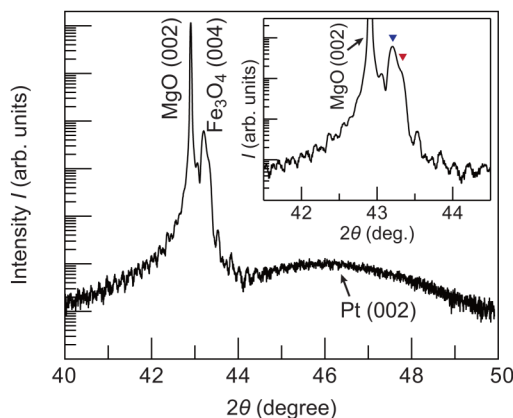
FIG. 1. $2\theta - \omega$ diffraction patterns of the $Fe_3O_4/Pt(\sim 2\,nm)/Fe_3O_4$ trilayer sample grown on the MgO (001) substrate. The inset shows the magnified view in the range of $41.50° < 2\theta < 44.50°$, where the Fe_3O_4 (004) diffraction peaks at lower and higher angles are marked by the blue and red triangles, respectively.

electron microscopy (TEM) and high-angle annular dark-field scanning TEM (HAADF-STEM) (see Fig. 2). The images of the overall sample cross section [Figs. 2(a) and 2(c)] show that each layer has a smooth surface and mostly uniform thickness. We confirmed that the bottom (first) Fe_3O_4 layer is epitaxially grown on the MgO (001) substrate and its interface is sharp [see Fig. 2(d) and its clear contrast change at the Fe_3O_4/MgO interface]. The Pt layer formed on the first Fe_3O_4 layer also shows epitaxial growth with the [001] orientation [see Figs. 2(g) and 2(h)]. Subsequently, the top (second) Fe_3O_4 layer is also found to grow epitaxially on the Pt (001) layer with keeping high crystallization. These results ensure full epitaxial growth from the substrate to the top Fe_3O_4 layer, consistent with the XRD result.

From the high resolution (HR) HAADF-STEM images shown in Figs. 2(g) and 2(h), we notice that there exists intermediate brightness regions and soft undulation between the Pt and Fe_3O_4 interface, indicating that the Pt film may be discontinuous and/or that the Pt/Fe_3O_4 interface may not be atomically sharp. In fact, the HR-TEM image in Fig. 2(b) captures a discontinuous region of Pt, and also the STEM images in Figs. 2(c) and 2(f) indicate that the Pt film consists of clusterlike structures due to the granular-type growth of Pt. To clarify the origin of the intermediate brightness regions and soft undulation at the Pt/Fe_3O_4 interface in more detail, we fabricated a $Fe_3O_4/Pt(10\,nm)/Fe_3O_4$ sample; owing to the Pt film much thicker than the previous sample, we can examine the interfacial property without considering the effect of discontinuity of the Pt film. Figure 3(a) shows the HR-TEM bright field image of the interface between the 10-nm-thick Pt and Fe_3O_4 formed on a MgO substrate. We found that in the vicinity of the Pt/Fe_3O_4 interface, there are small lobules (nanograins) (< 1 nm) consisting of Fe_3O_4 and Pt that are alternately formed with each other along the lateral direction [see Fig. 3(a)]. Figure 3(b) shows a corresponding HR-HAADF-STEM image of the same sample. The alternate Fe_3O_4 and Pt lobules observed by HR-TEM [Fig. 3(a)] were found to appear as intermediate brightness and soft undulation in the region around 1.5–2 unit cells of the Pt film from the interface. To evaluate the interfacial Fe, O, and Pt elements profile, we carried out electron energy loss spectroscopy (EELS) and energy dispersive X-ray spectroscopy (EDX).[21] As shown in Fig. 3(c), around the interface, the element profile varies in the range of 0.75–1 nm and there are finite Fe and O contributions in the Pt layer. This can be due to the overlap of the interfacial Fe_3O_4 and Pt lobules [Fig. 3(a)] existing along the depth direction (i.e., perpendicular to the cross plane) or simply due to some Pt, Fe, and O diffusion. Unfortunately, we cannot separate these two possible contributions in the present analysis.

3. Electric and magnetic properties of Fe_3O_4

We also characterized the electric and magnetic properties of the Fe_3O_4 film by four-probe conductivity measurements and vibrating sample magnetometry, respectively. We found that the electrical conductivity σ of our Fe_3O_4 film is $\sim 1.4 \times 10^2 / \Omega$ cm, being consistent with the literature value,[65] which confirms the metallic behavior of the Fe_3O_4 film at room temperature. As shown in Fig. 4(a), as the temperature T decreases, σ was found to monotonically decrease. Moreover, below ~ 110 K, σ dramatically
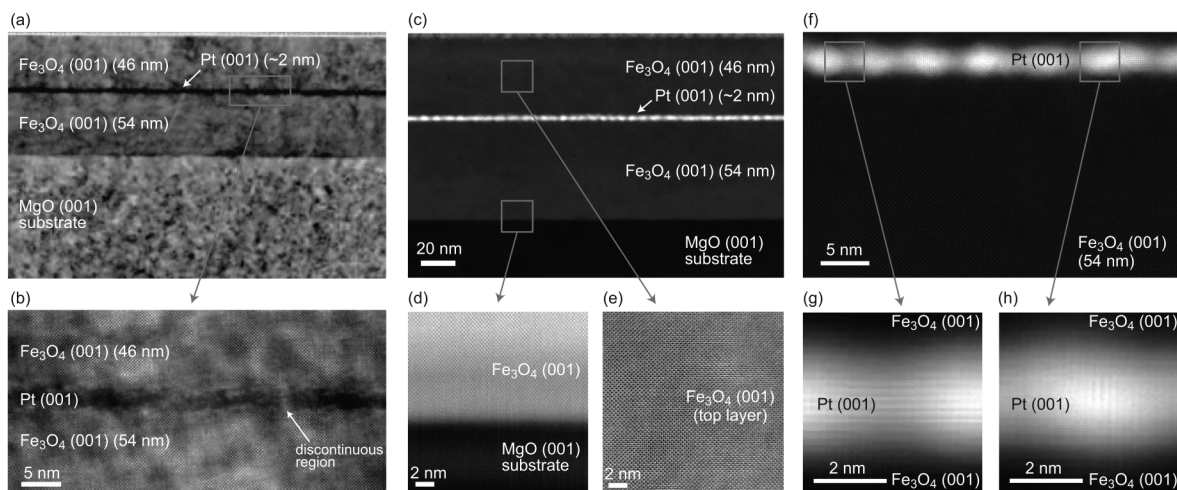
**FIG. 2.** (a) and (b) Cross-sectional TEM images of the $Fe_3O_4/Pt(\sim 2\,nm)/Fe_3O_4//MgO$ sample for (a) the overall sample cross section and for (b) the $Fe_3O_4/Pt/Fe_3O_4$ interfaces with higher resolution. (c)–(h) HAADF-STEM images of the $Fe_3O_4/Pt/Fe_3O_4//MgO$ sample for (c) the overall sample cross section, for (d) the Fe_3O_4/MgO interface, for (e) the top Fe_3O_4 layer grown on the Pt layer, and for (f) the $Fe_3O_4/Pt/Fe_3O_4$ interfaces. The HR-HAADF-STEM images focusing on the vicinity of the $Fe_3O_4/Pt/Fe_3O_4$ interfaces are shown in (g) and (h). The TEM lamellae specimen was prepared using a focused ion beam. HAADF-STEM was carried out with a probe-aberration-corrected FEI Titan 60-300 operated at 300 kV.

decreases with decreasing T, showing the metal-insulator (Verwey) transition of Fe_3O_4.[40,65] Figure 4(b) shows the observed magnetic field H dependence of the magnetization M (M-H curve) for the $Fe_3O_4/Pt(\sim 2\,nm)/Fe_3O_4$ sample at $T = 300\,K$. The saturation M value was found to be $333\,emu/cm^3$, smaller than the bulk value of

$480\,emu/cm^3$,[60] which can be attributed to the higher density of antiphase boundaries of PLD-grown Fe_3O_4 films.[63,66] From M-T curves, the Verwey transition temperature (T_V) of our Fe_3O_4 films was determined to be $\sim 114\,K$ [see the inset in Fig. 4(b)], consistent with the literature values for Fe_3O_4 films with similar thickness.[63]
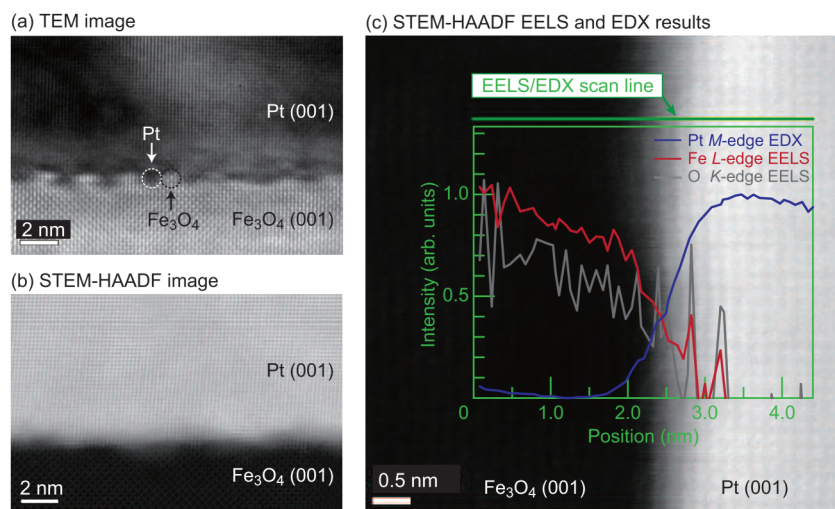
FIG. 3. (a) HR-TEM and (b) HR-HAADF-STEM images around the Pt/Fe_3O_4 interface of the $Fe_3O_4/Pt(10\,nm)/Fe_3O_4//MgO$ sample. In (a), the observed small Fe_3O_4 and Pt lobules (nanograins) are marked by dashed circles. (c) EDX line scan for Pt (M-edge, blue solid line) and EELS line scans for Fe (L-edge, red solid line) and O (K-edge, gray solid line) across the interface indicated by the green solid line.[21] The EELS measurement was done by using a probe-corrected Titan G2, where the beam diameter is around $0.1 - 0.15\,nm$, ensuring enough resolution to probe the elements at the interface. Besides, by diffraction analysis, the incident electron beam was directed to be orthogonal to the film cross plane. This ensures that the observed signal comes from the parallel plane and does not come from crosswise planes that may result in an artificial composition-mixed signal.
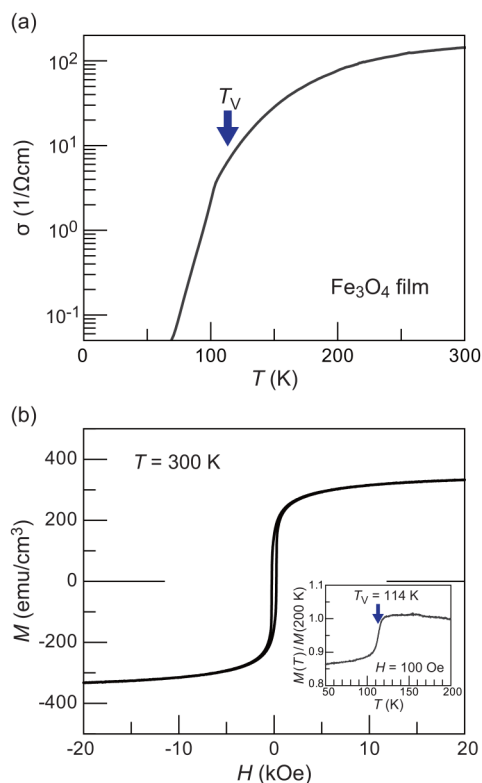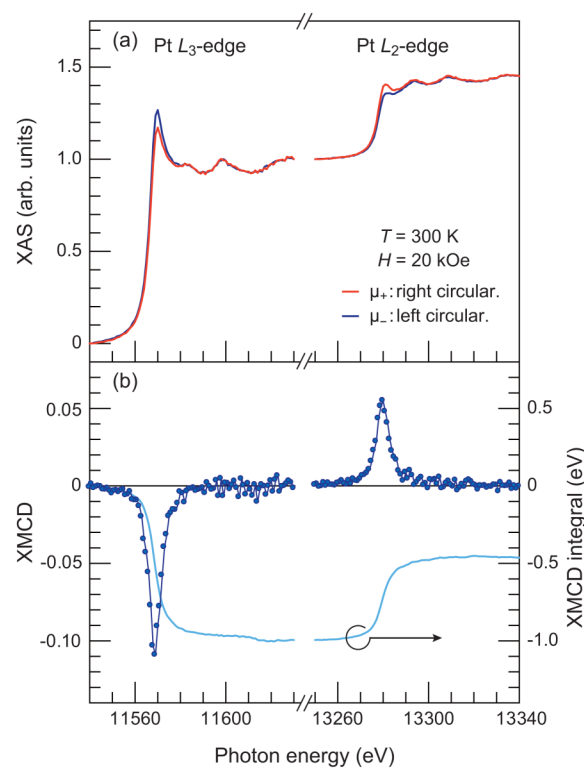
FIG. 4. (a) T dependence of the electrical conductivity σ for a 40-nm-thick Fe_3O_4 (001) film grown on a MgO (001) substrate. (b) M-H curve of the $Fe_3O_4/Pt(\sim 2\,nm)/Fe_3O_4$ sample at $T = 300\,K$, measured with a vibrating sample magnetometer. The inset to (b) shows the normalized M-T curve measured at $H = 100\,Oe$. The external field of 100 Oe is smaller than the coercive field of Fe_3O_4 ($H_c \sim 250\,Oe$). The T_V value can be determined via this measurement, since, with decreasing T, the M value at $H < H_c$ steeply decreases when the Verwey transition occurs at $T = T_V$ due to the enhancement of H_c (magnetic anisotropy).[65,66]

FIG. 5. (a) The normalized XAS for the Pt $L_{3,2}$-edges of the $Fe_3O_4/Pt(\sim 2\,nm)/Fe_3O_4$ sample at $T = 300\,K$ and $H = 20\,kOe$. The XAS edge jump, defined as the difference in the XAS intensity between 11 540 eV (13 250 eV) and 11 630 eV (13 340 eV), is normalized to 1 (2.22^{-1}) for the L_3-edge (L_2-edge) according to Refs. 67 and 68. The XAS offset value for the L_3-edge (L_2-edge) is set to be 0 (1).[29,31,51,68] μ_+ (μ_-) represents the XAS obtained with the right (left) circularly-polarized X-rays. (b) The XMCD spectra (blue circles with solid lines) and their integral (light-blue solid lines) for the Pt $L_{3,2}$-edges of the $Fe_3O_4/Pt/Fe_3O_4$ sample.

B. XAS, XMCD, and ESM results at $T = 300\,K$

Now, we present the results on the X-ray absorption of the $Fe_3O_4/Pt(\sim 2\,nm)/Fe_3O_4$ sample at $T = 300\,K$ and $H = 20\,kOe$. Figure 5(a) shows the measured XAS for the Pt $L_{3,2}$-edges with right (μ_+) and left (μ_-) circularly-polarized X-rays, where the XAS edge jump is normalized to 1 (2.22^{-1}) for the L_3-edge (L_2-edge).[67,68] The whiteline intensity, the ratio of the absorption maximum at the L_3-edge to the edge jump, of $(\mu_+ + \mu_-)/2$ is estimated to be ~ 1.25, comparable to that for a Pt foil.[31,68] Oscillation behaviors were observed in the extended X-ray absorption fine structure (EXAFS) region. These are characteristics of metallic Pt,[31] ensuring the quality of our Pt film.

The XAS shown in Fig. 5(a) exhibits a clear helicity dependence. Figure 5(b) shows the corresponding XMCD spectra ($\mu_+ - \mu_-$) at $T = 300\,K$ and $H = 20\,kOe$. The sign of the XMCD signal is negative at the L_3-edge (11 569 eV) and positive at the L_2-edge (13 280 eV), consistent with Pt films having magnetic

moments parallel to H.[48,51] Significantly, the XMCD intensity of ~ 0.11 (0.055) at the L_3-edge (L_2-edge) with respect to the XAS edge jump is two orders of magnitude greater than that for a Pt foil,[68] in which only the Pauli paramagnetism of Pt appears. This result suggests that our Pt film sandwiched between the Fe_3O_4 films acquires considerable induced magnetic moments, a situation different from the previous reports in conventional Pt/magnetic-oxide systems[29,31–35] including the Pt(2 nm)/Fe_3O_4 system reported in Ref. 37.

To check the H dependence of the induced moments in Pt, we measured the ESM curve at the Pt L_3-edge. We found that the XMCD magnitude increases with increasing H from zero and saturates at $H \sim 5\,kOe$ and that the sign of the XMCD signal changes by reversing the H direction (see Fig. 6). The ESM curve is well consistent with the ferromagnetic M-H curve for the Fe_3O_4 layers (see the inset to Fig. 6), suggesting that the observed XMCD signal is due to the Pt ferromagnetism whose magnetization process is governed by the Fe_3O_4 layers.
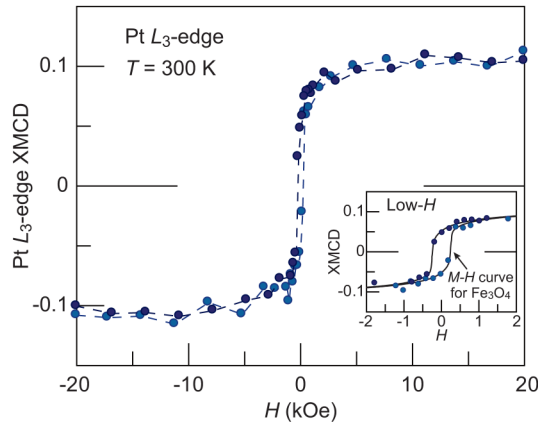
FIG. 6. The ESM curve at the Pt L_3-edge of the $Fe_3O_4/Pt(\sim 2\,nm)/Fe_3O_4$ sample at $T = 300\,K$ and the fixed photon energy of $11\,569\,eV$. The inset shows the comparison between the ESM curve (dark-blue and blue circles) and the M-H curve for the Fe_3O_4 layers (black solid lines, in arbitrary units) in the range of $|H| < 2\,kOe$.

The observed XMCD intensity, or the induced magnetic moment, in the present $Fe_3O_4/Pt/Fe_3O_4$ sample is quite large. The Pt ferromagnetic moment value at $H = 20\,kOe$ was estimated to be $m_{tot} = m_{orb} + m_{spin} = 0.39 \pm 0.05\,\mu_B$ by XMCD

sum-rule analysis,[48,69,70] where $m_{orb} = 0.05 \pm 0.01\,\mu_B$ and $m_{spin} = 0.34 \pm 0.05\,\mu_B$ are the orbital and (effective) spin magnetic moments, respectively (see Sec. A in the supplementary material for details on the sum-rule analysis). The ratio of the orbital-to-spin magnetic moment is $m_{orb}/m_{spin} = 0.15 \pm 0.02$. Interestingly, the m_{tot} value is comparable to or greater than those in Pt/3d-ferromagnetic-metal (Fe, Ni, Co, and $Ni_{81}Fe_{19}$) junction and $L1_0$-FePt alloy systems (see Table I). For example, the m_{tot} values in the Pt(2 and 1 nm)/Co bilayers were, respectively, reported to be $0.16\,\mu_B$ and $0.28\,\mu_B$,[48] which are smaller than that in our $Fe_3O_4/Pt(\sim 2\,nm)/Fe_3O_4$ trilayer system. Also, the m_{tot} value in the Pt(1 nm)/$Ni_{81}Fe_{19}$ superlattice (SL) system, where the Pt film is sandwiched by ferromagnetic $Ni_{81}Fe_{19}$ layers in a similar way as our sample system, was estimated to be $0.27\,\mu_B$,[53] again giving a value smaller than the present one. In contrast, the m_{orb}/m_{spin} ratio is almost the same as those in the previous Pt/3d-ferromagnetic-metal junctions (see Table I).

C. Temperature dependence of XMCD

We carried out systematic measurements on the T dependence of the XMCD using the same $Fe_3O_4/Pt(\sim 2\,nm)/Fe_3O_4$ sample. Figure 7(a) shows the Pt L_3-edge XMCD spectra at $H = 12\,kOe$ at several T values (left vertical axis) and their integrals (right vertical axis) and Fig. 7(b) shows the XMCD-integral values as a function of T. We found that the XMCD amplitude monotonically increases with decreasing T [see Fig. 7(a)]. The XMCD-integral value at the

TABLE I. Comparison of induced Pt magnetic moments at room temperature in various junction systems comprising Pt and magnetic materials and also $L1_0$-FePt alloys.[71] M_{FM} represents the volume magnetization value of the ferro(ferri)magnetic (FM) layers. The M_{FM} value for $L1_0$-FePt alloys is obtained by calculating the Fe contribution to the volume magnetization of $L1_0$-FePt.

System	Method	m_{tot} (μ_B/Pt)	m_{spin} (μ_B/Pt)	m_{orb} (μ_B/Pt)	m_{orb}/m_{spin}	M_{FM} (emu/cm^3)	Comment on Pt fabrication
$Fe_3O_4/Pt(\sim 2\,nm)/Fe_3O_4$	XMCD	0.39	0.34	0.050	0.15	333	High-T growth
$Fe_3O_4/Pt(\sim 5\,nm)/Fe_3O_4$	XMCD	0.36	0.32	0.043	0.14	333	High-T growth
Pt(2 nm)/Co[48]	XMCD	0.16	0.14	0.020	0.14	1440[60]	
Pt(1 nm)/Co[48]	XMCD	0.28	0.24	0.037	0.15	1440[60]	
Pt/Fe interface[32]	XRMR	0.6				1710[60]	
Pt/$Ni_{81}Fe_{19}$ interface[52]	XRMR	0.22				830[60]	
Pt/Ni interface[52]	XRMR	0.08				488[60]	
Pt(1 nm)/$Ni_{81}Fe_{19}$ SL[53]	XMCD	0.27			0.18	830[60]	
$L1_0$-FePt alloy[55]	XMCD	0.38	0.30	0.075	0.25	840[55]	
$L1_0$-FePt alloy[56]	XMCD	0.32	0.28	0.039	0.14	840[56]	
Pt(1.5 nm)/$Y_3Fe_5O_{12}$[30]	XMCD	0.054	0.044	0.010	0.23	140[30]	
Pt(3 nm)/$Y_3Fe_5O_{12}$[29]	XMCD	<0.003				110[29]	
Pt(2 nm)/Fe_3O_4[37]	XMCD	<0.005				$\sim$500[37]	Room-T growth
Pt(7 nm)/$CoFe_2O_4$[35]	XMCD	<0.002				160[35]	
Pt(2 nm)/$CoFe_2O_4$[37]	XMCD	<0.005				$\sim$200[37]	Room-T growth
Pt(4 nm)/$CoFe_2O_4$[38]	XMCD	<0.01				$\sim$340[38]	Room-T growth
Pt(4 nm)/$CoFe_2O_4$[38]	XMCD	0.24				$\sim$340[38]	High-T growth
Pt(2 nm)/$MnFe_2O_4$[37]	XMCD	<0.005				$\sim$100[37]	Room-T growth
Pt(2 nm)/$NiFe_2O_4$[37]	XMCD	<0.005				$\sim$70[37]	Room-T growth
Pt/$NiFe_2O_4$ interface[32]	XRMR	<0.02				$\sim$230[32]	
Pt/$NiFe_2O_4$ interface[33]	XRMR	<0.04				244[33]	
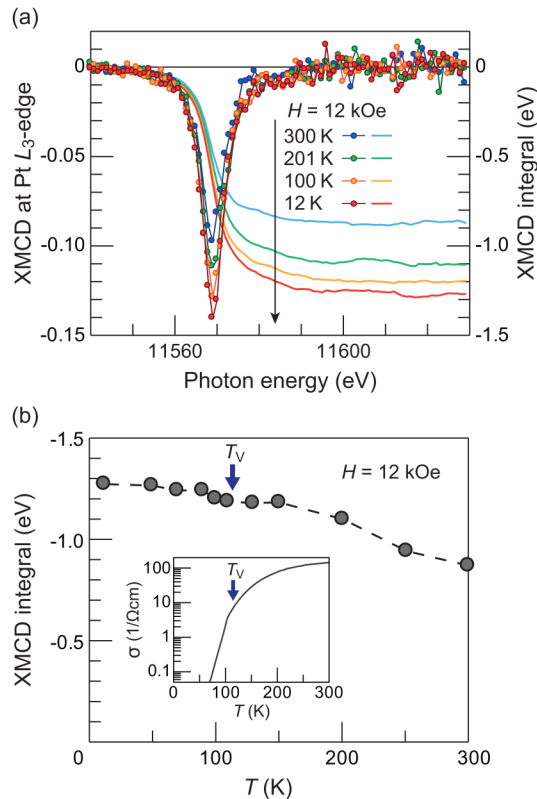
FIG. 7. (a) The XMCD spectra for the Pt L_3-edge of the Fe_3O_4/Pt($\sim$2 nm)/Fe_3O_4 sample (left vertical axis) and their integral (right vertical axis) measured at $H = 12$ kOe at several T values. (b) T dependence of the XMCD integral at $H = 12$ kOe. The inset to (b) shows the T dependence of σ of the Fe_3O_4 film, which is the same as that shown in Fig. 4(a).

FIG. 8. The ESM curve at the Pt L_3-edge of the Fe_3O_4/Pt($\sim$2 nm)/Fe_3O_4 sample at $T = 12$ K (dark-red and red circles with dashed lines). For comparison, the ESM curve measured at $T = 300$ K is also plotted (dark-blue and blue circles with dashed lines). The inset shows the comparison between the ESM curve at $T = 12$ K (dark-red and red circles) and M-H curve for the Fe_3O_4 layers at $T = 10$ K (black solid lines, in arbitrary units) in the range of $|H| < 2$ kOe.

lowest temperature (12 K) increases by a factor of $\sim$1.4 compared to that at 300 K. Interestingly, this enhancement is more prominent than that of magnetization of Fe_3O_4 ($\sim$1.05 in the same T range[72]). Furthermore, the metal-insulator transition of Fe_3O_4 does not affect the present Pt ferromagnetism, since no meaningful change of the XMCD signal was observed at around $T_V \sim 114$ K [see Fig. 7(b)].

Figure 8 shows the ESM curve at the Pt L_3-edge at 12 K (dark-red and red circles) and the comparison of the ESM curve with that at 300 K (dark-blue and blue circles). We found that the amplitude of the ESM curve at 12 K is greater than that at 300 K, consistent with the XMCD spectra shown in Fig. 7(a). We also found that the coercivity of the ESM curve enhances at 12 K compared to that at 300 K, in agreement with that of the M-H curve of the Fe_3O_4 layers (see the inset of Fig. 8), which is due to the increase of the magnetic anisotropy of Fe_3O_4 below T_V.[66]

From the integrated XAS and XMCD measured at $T = 12$ K and $H = 12$ kOe, the Pt ferromagnetic moment value under this condition was estimated to be $m_{tot} = m_{orb} + m_{spin} = 0.52 \pm 0.06 \mu_B$,

where $m_{orb} = 0.06 \pm 0.01 \mu_B$ and $m_{spin} = 0.46 \pm 0.06 \mu_B$ (see Sec. B in the supplementary material for details, in which the XAS and XMCD full spectra for the Pt $L_{3,2}$-edges at 12 K and 12 kOe are shown). As expected from the XMCD data shown in Fig. 7(b), the m_{tot} value at 12 K increases by a factor of $\sim$1.4 compared to that at 300 K. On the other hand, the ratio of the orbital-to-spin magnetic moment is $m_{orb}/m_{spin} = 0.13 \pm 0.01$, which agrees with that estimated at 300 K within the experimental error. The m_{tot} value at 12 K is more than two times greater than that in Pt/Ni junction systems at similar temperatures[44–46] and is comparable to (or even slightly greater than) that of $L1_0$-FePt alloys ($= 0.45 \pm 0.03 \mu_B$/Pt at 15 K[54]).

D. Effect of Pt thickness on XMCD

To reveal the effect of Pt thickness t_{Pt} on the XMCD amplitude, we also measured XMCD using a Fe_3O_4/Pt($\sim$5 nm)/Fe_3O_4 sample at $T = 300$ K and 12 K, where the 2-nm-thick Pt film is replaced with the thicker one ($t_{Pt} \sim 5$ nm). As shown in Fig. 9(a), clear XMCD signals were observed, whose intensity at 12 K is larger than that at 300 K, consistent with the $t_{Pt} \sim 2$ nm sample. From the integrated XAS and XMCD measured at $T = 300$ K, the Pt ferromagnetic moment value of the present $t_{Pt} \sim 5$ nm sample was estimated to be $m_{tot} = m_{orb} + m_{spin} = 0.36 \pm 0.04 \mu_B$, where $m_{orb} = 0.043 \pm 0.007 \mu_B$ and $m_{spin} = 0.32 \pm 0.04 \mu_B$. These values are comparable to those for the $t_{Pt} \sim 2$ nm sample at $T = 300$ K within the experimental error (see also Table I). The Pt thickness dependence result is distinct from the previous XMCD study at the Pt $L_{3,2}$-edges of Pt(t_{Pt})/Co samples,[48] where the substantial decrease of the XMCD signal with increasing t_{Pt} is observed. In Ref. 48, this feature is explained by the model that the
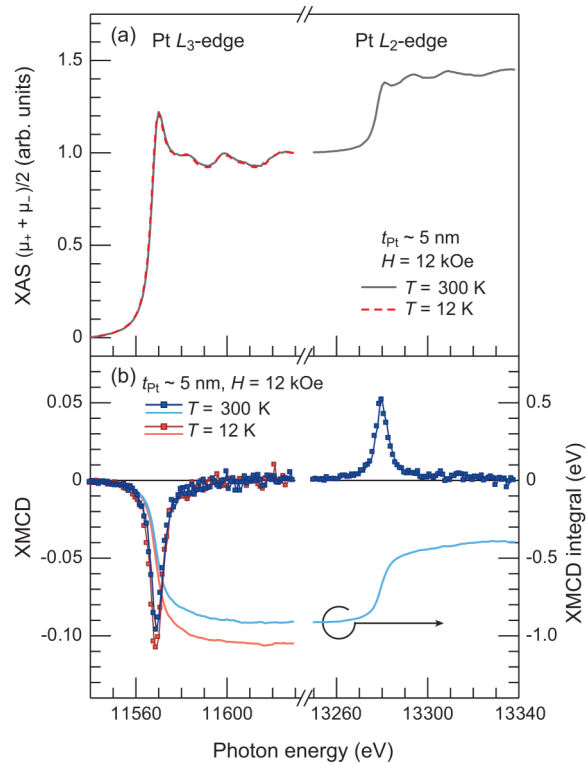
FIG. 9. (a) The normalized XAS $[(\mu_+ + \mu_-)/2]$ for the Pt $L_{3,2}$-edges of the Fe$_3$O$_4$/Pt($\sim$5 nm)/Fe$_3$O$_4$ sample at $T = 300$ K and $H = 12$ kOe (gray solid lines). (b) The XMCD spectra (blue circles with solid lines) and the corresponding XMCD integrals (light-blue solid lines) at $T = 300$ K and $H = 12$ kOe for the Pt $L_{3,2}$-edges of the Fe$_3$O$_4$/Pt($\sim$5 nm)/Fe$_3$O$_4$ sample. In (a) and (b), the normalized XAS and the XMCD spectrum/integral for the Pt L_3-edge of the Fe$_3$O$_4$/Pt($\sim$ 5 nm)/Fe$_3$O$_4$ sample measured at $T = 12$ K are also plotted, respectively.

ferromagnetic Pt moment exponentially decreases with the distance from the interface, the decay length of which is estimated to be 0.41 nm.

E. Discussion on the large Pt ferromagnetic moment in Fe$_3$O$_4$/Pt/Fe$_3$O$_4$

The giant Pt ferromagnetic moment m_{tot} value in the present Fe$_3$O$_4$/Pt/Fe$_3$O$_4$ systems is unconventional in the light of the volume magnetization (M_{FM}) value of the Fe$_3$O$_4$ layers. In the previous reports for the Pt/3d-ferromagnetic-metal junction systems at room temperature, the proximity-induced m_{tot} values tend to scale with the M_{FM} values of the ferromagnetic layers (see Table I for 300 K). In fact, the m_{tot} vs M_{FM} scaling was recently confirmed for Pt/Ni$_{1-x}$Fe$_x$ and Pt/Co$_{1-x}$Fe$_x$ bilayers via XRMR measurements in Ref. 73. However, our XMCD result clearly deviates from this tendency; although the M_{FM} value of the Fe$_3$O$_4$ layer is much smaller than those of the 3d-ferromagnetic-metal layers as shown in Table I, the m_{tot} value in our systems is comparable to or greater

than those in the Pt/3d-ferromagnetic-metal systems. Such deviation may become more outstanding at the lowest temperature (12 K); the m_{tot} value in the present Fe$_3$O$_4$/Pt($\sim$2 nm)/Fe$_3$O$_4$ system increases by a factor of $\sim$1.4 compared to that at 300 K, while the magnetization of Fe$_3$O$_4$ increases only by $\sim$1.05 in the same T range, as mentioned in Sec. III C.

Our results are distinct also from the recent XMCD results in the Pt(2 nm)/Fe$_3$O$_4$ film reported by Collet et al. in Ref. 37, in which the XMCD signal was undetectably small at the temperatures above and below T_V (290 and 10 K). Here, their Pt film was formed with room-temperature sputtering, while our Pt films were fabricated with high-temperature sputtering ($\sim$480 °C). This difference in the fabrication process may affect the resultant XMCD signal.

Very recently, Vasili et al.[38] reported systematic XMCD results in Pt(4 nm)/CoFe$_2$O$_4$ films, where the Pt deposition temperature was varied. They observed a large XMCD signal in a Pt/CoFe$_2$O$_4$ sample when the Pt film is formed at a high temperature of 400 °C, whose Pt ferromagnetic moment value was determined to be $m_{tot} = 0.24\,\mu_B$.[38] This is in contrast to the absence of the XMCD signal in the other Pt/CoFe$_2$O$_4$ sample, where the Pt film is formed at room temperature.[38] Through systematic XAS and XMCD measurements at the Fe and Co $L_{3,2}$-edges in both the total electron yield (TEY) and fluorescence yield (FY) modes and also STEM-EELS observations, they found that, in the high-T grown Pt/CoFe$_2$O$_4$ sample, the XAS and XMCD spectra for the (surface-sensitive) TEY mode contain metallic Fe and Co signals and also found that the Pt/CoFe$_2$O$_4$ interface becomes less sharper than that deposited at room T. From these results, they concluded that, in the high-T grown Pt/CoFe$_2$O$_4$ sample, there are an interfacial Pt-(Co, Fe) alloying and/or a (Co, Fe)-interdiffusion into the Pt layer, which are negligible for the room-T grown one.[38] The feature results in the large (negligibly small) XMCD for the high-T (room-T) grown sample.

Based on the above arguments, the large XMCD signal and large Pt ferromagnetic moment observed in the present Fe$_3$O$_4$/Pt/Fe$_3$O$_4$ systems prepared at a high temperature can be interpreted in terms of the possible heat-induced Fe interdiffusion into the Pt layer and Pt-Fe alloying (cannot be explained by the conventional interfacial magnetic proximity-induced Pt ferromagnetism). This scenario is also supported by our experimental facts, as shown below. (1) The Pt/Fe$_3$O$_4$ interfaces are not atomically sharp and the interdiffusion is likely to be present (Sec. III A 2). (2) The Pt ferromagnetic moment m_{tot} increases more strongly than the T dependence of M of Fe$_3$O$_4$ (i.e., the present m_{tot} does not correlate with the M intensity of Fe$_3$O$_4$, different from the previous reports) (Secs. III C and III E). (3) The m_{tot} value remains almost unchanged (decreases by only 10%) by increasing the Pt thickness from 2 to 5 nm, which does not agree with the proximity-induced Pt ferromagnetism scenario and is indeed different from the previous Pt thickness dependent XMCD results in Pt/Co bilayers, where the Pt films are deposited at room temperature[48] (Sec. III D). Furthermore, we confirmed that the XAS and XMCD results in the TEY mode for the Fe $L_{3,2}$-edges of our Pt($\sim$5 nm)/Fe$_3$O$_4$/Pt($\sim$2 − 3 nm)/Fe$_3$O$_4$ reasonably agree with the results in the high-T grown Pt/CoFe$_2$O$_4$ reported by Vasili et al.,[38] indicating the presence of metallic Fe states in our Pt layer (see Sec. C in the supplementary material for details). The result

also supports our present scenario on the origin of the large induced Pt ferromagnetism in the $Fe_3O_4/Pt/Fe_3O_4$ systems. Nevertheless, further work would be needed to obtain a complete physical picture of the present large Pt ferromagnetism.

IV. CONCLUSION

To summarize, by means of XMCD, we have investigated the induced Pt ferromagnetism in $Fe_3O_4/Pt(t_{Pt} \sim 2$ and $5\,nm)/Fe_3O_4$ epitaxial trilayer films at various temperatures, covering the metal-insulator transition temperature of Fe_3O_4 ($T_V \sim 114\,K$). The result shows the appearance of the large induced Pt ferromagnetic moment m_{tot} of $0.39\,\mu_B$ ($0.36\,\mu_B$) at $300\,K$ and $0.52\,\mu_B$ at $12\,K$ for the $t_{Pt} = 2\,nm$ ($5\,nm$) sample. The value does not follow the conventional scaling on m_{tot} vs volume magnetization M_{FM} of the magnetic layers. The appearance of the large XMCD (Pt ferromagnetism) in the present $Fe_3O_4/Pt/Fe_3O_4$ systems prepared at a high temperature of $480\,°C$ is different from the absence of the measurable XMCD in Pt/Fe_3O_4 in the recent report in Ref. 37, where the Pt film is formed at room temperature. Our results can be interpreted in terms of the possible heat-induced Fe interdiffusion into the Pt layer and Fe-Pt alloying due to its high-temperature deposition.

Recently, some of the present authors found measurable anomalous Nernst signals in $Fe_3O_4/Pt/Fe_3O_4$ epitaxial trilayers in a wide temperature range even below T_V of Fe_3O_4. The result is attributed to the magnetized Pt due to the possible Fe interdiffusion into the Pt layer by the high-temperature Pt deposition, in a similar way to the present study.[21] We anticipate that our comprehensive temperature, magnetic field, and Pt thickness dependent XMCD results provide useful information to elucidate the origin of their observation.[21]

SUPPLEMENTARY MATERIAL

See the supplementary material for the details of XMCD sum-rule analysis and XAS and XMCD full spectra for the Pt $L_{3,2}$-edges of $Fe_3O_4/Pt(\sim2\,nm)/Fe_3O_4$ at $T = 12\,K$ and for the Fe $L_{3,2}$-edges of $Pt(\sim5\,nm)/Fe_3O_4/Pt(\sim2-3\,nm)/Fe_3O_4$ sample at room temperature.

ACKNOWLEDGMENTS

REFERENCES

[1]F. Hellman, A. Hoffmann, Y. Tserkovnyak, G. S. D. Beach, E. E. Fullerton, C. Leighton, A. H. MacDonald, D. C. Ralph, D. A. Arena, H. A. Dürr, P. Fischer, J. Grollier, J. P. Heremans, T. Jungwirth, A. V. Kimel, B. Koopmans, I. N. Krivorotov, S. J. May, A. K. Petford-Long, J. M. Rondinelli, N. Samarth, I. K. Schuller, A. N. Slavin, M. D. Stiles, O. Tchernyshyov, A. Thiaville, and B. L. Zink, "Interface-induced phenomena in magnetism," Rev. Mod. Phys. **89**, 025006 (2017).

[2]K. Uchida, H. Adachi, T. Ota, H. Nakayama, S. Maekawa, and E. Saitoh, "Observation of longitudinal spin-Seebeck effect in magnetic insulators," Appl. Phys. Lett. **97**, 172505 (2010).

[3]K. Uchida, H. Adachi, T. Kikkawa, A. Kirihara, M. Ishida, S. Yorozu, S. Maekawa, and E. Saitoh, "Thermoelectric generation based on spin Seebeck effects," Proc. IEEE **104**, 1946 (2016); **104**, 1499 (2016).

[4]H. Nakayama, M. Althammer, Y.-T. Chen, K. Uchida, Y. Kajiwara, D. Kikuchi, T. Ohtani, S. Geprägs, M. Opel, S. Takahashi, R. Gross, G. E. W. Bauer, S. T. B. Goennenwein, and E. Saitoh, "Spin Hall magnetoresistance induced by a nonequilibrium proximity effect," Phys. Rev. Lett. **110**, 206601 (2013).

[5]Y.-T. Chen, S. Takahashi, H. Nakayama, M. Althammer, S. T. B. Goennenwein, E. Saitoh, and G. E. W. Bauer, "Theory of spin Hall magnetoresistance (SMR) and related phenomena," J. Phys. Condens. Matter **28**, 103004 (2016).

[6]A. Hoffmann, "Spin Hall effects in metals," IEEE Trans. Magn. **49**, 5172 (2013).

[7]J. Sinova, S. O. Valenzuela, J. Wunderlich, C. H. Back, and T. Jungwirth, "Spin Hall effects," Rev. Mod. Phys. **87**, 1213 (2015).

[8]M. Althammer, S. Meyer, H. Nakayama, M. Schreier, S. Altmannshofer, M. Weiler, H. Huebl, S. Geprägs, M. Opel, R. Gross, D. Meier, C. Klewe, T. Kuschel, J.-M. Schmalhorst, G. Reiss, L. Shen, A. Gupta, Y.-T. Chen, G. E. W. Bauer, E. Saitoh, and S. T. B. Goennenwein, "Quantitative study of the spin Hall magnetoresistance in ferromagnetic insulator/normal metal hybrids," Phys. Rev. B **87**, 224401 (2013).

[9]S. Geprägs, A. Kehlberger, F. D. Coletta, Z. Qiu, E.-J. Guo, T. Schulz, C. Mix, S. Meyer, A. Kamra, M. Althammer, H. Huebl, G. Jakob, Y. Ohnuma, H. Adachi, J. Barker, S. Maekawa, G. E. W. Bauer, E. Saitoh, R. Gross, S. T. B. Goennenwein, and M. Kläui, "Origin of the spin Seebeck effect in compensated ferrimagnets," Nat. Commun. **7**, 10452 (2016).

[10]D. Meier, T. Kuschel, L. Shen, A. Gupta, T. Kikkawa, K. Uchida, E. Saitoh, J.-M. Schmalhorst, and G. Reiss, "Thermally driven spin and charge currents in thin $NiFe_2O_4/Pt$ films," Phys. Rev. B **87**, 054421 (2013).

[11]M. Isasa, A. Bedoya-Pinto, S. Vélez, F. Golmar, F. Sánchez, L. E. Hueso, J. Fontcuberta, and F. Casanova, "Spin Hall magnetoresistance at $Pt/CoFe_2O_4$ interfaces and texture effects," Appl. Phys. Lett. **105**, 142402 (2014).

[12]T. Niizeki, T. Kikkawa, K. Uchida, M. Oka, K. Z. Suzuki, H. Yanagihara, E. Kita, and E. Saitoh, "Observation of longitudinal spin-Seebeck effect in cobalt-ferrite epitaxial thin films," AIP Adv. **5**, 053603 (2015).

[13]E.-J. Guo, A. Herklotz, A. Kehlberger, J. Cramer, G. Jakob, and M. Kläui, "Thermal generation of spin current in epitaxial $CoFe_2O_4$ thin films," Appl. Phys. Lett. **108**, 022403 (2016).

[14]A. Aqeel, N. Vlietstra, J. A. Heuver, G. E. W. Bauer, B. Noheda, B. J. van Wees, and T. T. M. Palstra, "Spin-Hall magnetoresistance and spin Seebeck effect in spin-spiral and paramagnetic phases of multiferroic $CoCr_2O_4$ films," Phys. Rev. B **92**, 224410 (2015).

[15]R. Ramos, T. Kikkawa, K. Uchida, H. Adachi, I. Lucas, M. H. Aguirre, P. Algarabel, L. Morellón, S. Maekawa, E. Saitoh, and M. R. Ibarra, "Observation of the spin Seebeck effect in epitaxial Fe_3O_4 thin films," Appl. Phys. Lett. **102**, 072413 (2013).

[16]S. M. Wu, J. Hoffman, J. E. Pearson, and A. Bhattacharya, "Unambiguous separation of the inverse spin Hall and anomalous Nernst effects within a ferromagnetic metal using the spin Seebeck effect," Appl. Phys. Lett. **105**, 092409 (2014).

[17]R. Ramos, T. Kikkawa, M. H. Aguirre, I. Lucas, A. Anadón, T. Oyake, K. Uchida, H. Adachi, J. Shiomi, P. A. Algarabel, L. Morellón, S. Maekawa, E. Saitoh, and M. R. Ibarra, "Unconventional scaling and significant enhancement of the spin Seebeck effect in multilayers," Phys. Rev. B **92**, 220407(R) (2015).

[18]A. Anadón, R. Ramos, I. Lucas, P. A. Algarabel, L. Morellón, M. R. Ibarra, and M. H. Aguirre, "Characteristic length scale of the magnon accumulation in Fe3O4/Pt bilayer structures by incoherent thermal excitation," Appl. Phys. Lett. **109**, 012404 (2016).

[19]R. Ramos, A. Anadón, I. Lucas, K. Uchida, P. A. Algarabel, L. Morellón, M. H. Aguirre, E. Saitoh, and M. R. Ibarra, "Thermoelectric performance of spin Seebeck effect in Fe3O4/Pt-based thin film heterostructures," APL Mater. **4**, 104802 (2016).

[20]R. Ramos, T. Kikkawa, A. Anadón, I. Lucas, K. Uchida, P. A. Algarabel, L. Morellón, M. H. Aguirre, E. Saitoh, and M. R. Ibarra, "Temperature dependence of the spin Seebeck effect in [Fe3O4/Pt]n multilayers," AIP Adv. **7**, 055915 (2017).

[21]R. Ramos, T. Kikkawa, A. Anadón, I. Lucas, T. Niizeki, K. Uchida, P. A. Algarabel, L. Morellón, M. H. Aguirre, M. R. Ibarra, and E. Saitoh, "Interface-induced anomalous Nernst effect in Fe3O4/Pt-based heterostructures," Appl. Phys. Lett. **114**, 113902 (2019).

[22]S. Y. Huang, X. Fan, D. Qu, Y. P. Chen, W. G. Wang, J. Wu, T. Y. Chen, J. Q. Xiao, and C. L. Chien, "Transport magnetic proximity effects in platinum," Phys. Rev. Lett. **109**, 107204 (2012).

[23]D. Qu, S. Y. Huang, J. Hu, R. Wu, and C. L. Chien, "Intrinsic spin Seebeck effect in Au/Y3Fe5O12," Phys. Rev. Lett. **110**, 067206 (2013).

[24]T. Kikkawa, K. Uchida, Y. Shiomi, Z. Qiu, D. Hou, D. Tian, H. Nakayama, X.-F. Jin, and E. Saitoh, "Longitudinal spin Seebeck effect free from the proximity Nernst effect," Phys. Rev. Lett. **110**, 067207 (2013).

[25]T. Kikkawa, K. Uchida, S. Daimon, Y. Shiomi, H. Adachi, Z. Qiu, D. Hou, X.-F. Jin, S. Maekawa, and E. Saitoh, "Separation of longitudinal spin Seebeck effect from anomalous Nernst effect: Determination of origin of transverse thermoelectric voltage in metal/insulator junctions," Phys. Rev. B **88**, 214403 (2013).

[26]B. F. Miao, S. Y. Huang, D. Qu, and C. L. Chien, "Absence of anomalous Nernst effect in spin Seebeck effect of Pt/YIG," AIP Adv. **6**, 015018 (2016).

[27]B. F. Miao, L. Sun, D. Wu, C. L. Chien, and H. F. Ding, "Magnetic scattering and spin-orbit coupling induced magnetoresistance in nonmagnetic heavy metal and magnetic insulator bilayer systems," Phys. Rev. B **94**, 174430 (2016).

[28]G. Y. Guo, Q. Niu, and N. Nagaosa, "Anomalous Nernst and Hall effects in magnetized platinum and palladium," Phys. Rev. B **89**, 214406 (2014).

[29]S. Geprägs, S. Meyer, S. Altmannshofer, M. Opel, F. Wilhelm, A. Rogalev, R. Gross, and S. T. B. Goennenwein, "Investigation of induced Pt magnetic polarization in Pt/Y3Fe5O12 bilayers," Appl. Phys. Lett. **101**, 262407 (2012).

[30]Y. M. Lu, Y. Choi, C. M. Ortega, X. M. Cheng, J. W. Cai, S. Y. Huang, L. Sun, and C. L. Chien, "Pt magnetic polarization on Y3Fe5O12 and magnetotransport characteristics," Phys. Rev. Lett. **110**, 147207 (2013).

[31]S. Geprägs, S. T. B. Goennenwein, M. Schneider, F. Wilhelm, K. Ollefs, A. Rogalev, M. Opel, and R. Gross, "Comment on 'Pt magnetic polarization on Y3Fe5O12 and magnetotransport characteristics,'" e-print arXiv:1307.4869 (2013).

[32]T. Kuschel, C. Klewe, J.-M. Schmalhorst, F. Bertram, O. Kuschel, T. Schemme, J. Wollschläger, S. Francoual, J. Strempfer, A. Gupta, M. Meinert, G. Götz, D. Meier, and G. Reiss, "Static magnetic proximity effect in Pt/NiFe2O4 and Pt/Fe bilayers investigated by X-ray resonant magnetic reflectivity," Phys. Rev. Lett. **115**, 097401 (2015).

[33]T. Kuschel, C. Klewe, P. Bougiatioti, O. Kuschel, J. Wollschläger, L. Bouchenoire, S. D. Brown, J.-M. Schmalhorst, D. Meier, and G. Reiss, "Static magnetic proximity effect in Pt layers on sputter-deposited Pt/NiFe2O4 and on Fe of various thicknesses investigated by XRMR," IEEE Trans. Magn. **52**, 4500104 (2016).

[34]H. Wu, Q. Zhang, C. Wan, S. S. Ali, Z. Yuan, L. You, J. Wang, Y. Choi, and X. Han, "Spin Hall magnetoresistance in CoFe2O4/Pt films," IEEE Trans. Magn. **51**, 4100104 (2015).

[35]M. Valvidares, N. Dix, M. Isasa, K. Ollefs, F. Wilhelm, A. Rogalev, F. Sánchez, E. Pellegrin, A. Bedoya-Pinto, P. Gargiani, L. E. Hueso, F. Casanova, and J. Fontcuberta, "Absence of magnetic proximity effects in magnetoresistive Pt/CoFe2O4 hybrid interfaces," Phys. Rev. B **93**, 214415 (2016).

[36]T. Kikkawa, M. Suzuki, J. Okabayashi, K. Uchida, D. Kikuchi, Z. Qiu, and E. Saitoh, "Detection of induced paramagnetic moments in Pt on Y3Fe5O12 via x-ray magnetic circular dichroism," Phys. Rev. B **95**, 214416 (2017).

[37]M. Collet, R. Mattana, J.-B. Moussy, K. Ollefs, S. Collin, C. Deranlot, A. Anane, V. Cros, F. Petroff, F. Wilhelm, and A. Rogalev, "Investigating magnetic proximity effects at ferrite/Pt interfaces," Appl. Phys. Lett. **111**, 202401 (2017).

[38]H. B. Vasili, M. Gamino, J. Gàzquez, F. Sánchez, M. Valvidares, P. Gargiani, E. Pellegrin, and J. Fontcuberta, "Magnetoresistance in hybrid Pt/CoFe2O4 bilayers controlled by competing spin accumulation and interfacial chemical reconstruction," ACS Appl. Mater. Interfaces **10**, 12031 (2018).

[39]K. Uchida, T. Kikkawa, T. Seki, T. Oyake, J. Shiomi, Z. Qiu, K. Takanashi, and E. Saitoh, "Enhancement of anomalous Nernst effects in metallic multilayers free from proximity-induced magnetism," Phys. Rev. B **92**, 054422 (2015).

[40]J. Stöhr and H. C. Siegmann, *Magnetism: From Fundamentals to Nanoscale Dynamics* (Springer, New York, 2006).

[41]S. W. Lovesey and S. P. Collins, *X-Ray Scattering and Absorption by Magnetic Materials* (Clarendon, Oxford, 1996).

[42]G. van der Laan and A. I. Figueroa, "X-ray magnetic circular dichroism—A versatile tool to study magnetism," Coord. Chem. Rev. **277–278**, 95 (2014).

[43]S. Macke and E. Goering, "Magnetic reflectometry of heterostructures," J. Phys. Condens. Matter **26**, 363201 (2014).

[44]F. Wilhelm, P. Poulopoulos, G. Ceballos, H. Wende, K. Baberschke, P. Srivastava, D. Benea, H. Ebert, M. Angelakeris, N. K. Flevaris, D. Niarchos, A. Rogalev, and N. B. Brookes, "Layer-resolved magnetic moments in Ni/Pt multilayers," Phys. Rev. Lett. **85**, 413 (2000).

[45]P. Poulopoulos, F. Wilhelm, H. Wende, G. Ceballos, K. Baberschke, D. Benea, H. Ebert, M. Angelakeris, N. K. Flevaris, A. Rogalev, and N. B. Brookes, "X-ray magnetic circular dichroic magnetometry on Ni/Pt multilayers," J. Appl. Phys. **89**, 3874 (2001).

[46]F. Wilhelm, P. Poulopoulos, H. Wende, A. Scherz, K. Baberschke, M. Angelakeris, N. K. Flevaris, and A. Rogalev, "Systematics of the induced magnetic moments in 5d layers and the violation of the third Hund's rule," Phys. Rev. Lett. **87**, 207202 (2001).

[47]H. Wende, "Recent advances in x-ray absorption spectroscopy," Rep. Prog. Phys. **67**, 2105 (2004).

[48]M. Suzuki, H. Muraoka, Y. Inaba, H. Miyagawa, N. Kawamura, T. Shimatsu, H. Maruyama, N. Ishimatsu, Y. Isohama, and Y. Sonobe, "Depth profile of spin and orbital magnetic moments in a subnanometer Pt film on Co," Phys. Rev. B **72**, 054430 (2005).

[49]A. Vlachos, V. Kapaklis, M. Angelakeris, E. Th. Papaioannou, F. Wilhelm, A. Rogalev, and P. Poulopoulos, "Induced magnetic moments of 4d and 5d elements in thin films and multilayers by X-ray magnetic circular dichroism," J. Surf. Interface Mater. **2**, 8 (2014).

[50]A. I. Figueroa, J. Bartolomé, L. M. García, F. Bartolomé, O. Bunău, J. Stankiewicz, L. Ruiz, J. M. González-Calbet, F. Petroff, C. Deranlot, S. Pascarelli, P. Bencok, N. B. Brookes, F. Wilhelm, A. Smekhova, and A. Rogalev, "Structural and magnetic properties of granular Co-Pt multilayers with perpendicular magnetic anisotropy," Phys. Rev. B **90**, 174421 (2014).

[51]A. Rogalev and F. Wilhelm, "Magnetic circular dichroism in the hard X-ray range," Phys. Met. Metallogr. **116**, 1285 (2015).

[52]C. Klewe, T. Kuschel, J.-M. Schmalhorst, F. Bertram, O. Kuschel, J. Wollschläger, J. Strempfer, M. Meinert, and G. Reiss, "Static magnetic proximity effect in Pt/Ni1−xFex bilayers investigated by x-ray resonant magnetic reflectivity," Phys. Rev. B **93**, 214440 (2016).

[53]M. Caminale, A. Ghosh, S. Auffret, U. Ebels, K. Ollefs, F. Wilhelm, A. Rogalev, and W. E. Bailey, "Spin pumping damping and magnetic proximity effect in Pd and Pt spin-sink layers," Phys. Rev. B **94**, 014414 (2016).

[54]C. Antoniak, J. Lindner, M. Spasova, D. Sudfeld, M. Acet, M. Farle, K. Fauth, U. Wiedwald, H.-G. Boyen, P. Ziemann, F. Wilhelm, A. Rogalev, and S. Sun, "Enhanced orbital magnetism in $Fe_{50}Pt_{50}$ nanoparticles," Phys. Rev. Lett. **97**, 117201 (2006).

[55]S. Miwa, M. Suzuki, M. Tsujikawa, K. Matsuda, T. Nozaki, K. Tanaka, T. Tsukahara, K. Nawaoka, M. Goto, Y. Kotani, T. Ohkubo, F. Bonell, E. Tamura, K. Hono, T. Nakamura, M. Shirai, S. Yuasa, and Y. Suzuki, "Voltage controlled interfacial magnetism through platinum orbits," Nat. Commun. **8**, 15848 (2017).

[56]K. Ikeda, T. Seki, G. Shibata, T. Kadono, K. Ishigami, Y. Takahashi, M. Horio, S. Sakamoto, Y. Nonaka, M. Sakamaki, K. Amemiya, N. Kawamura, M. Suzuki, K. Takanashi, and A. Fujimori, "Magnetic anisotropy of $L1_0$-ordered FePt thin films studied by Fe and Pt $L_{3,2}$-edges x-ray magnetic circular dichroism," Appl. Phys. Lett. **111**, 142402 (2017).

[57]Z. Szotek, W. M. Temmerman, D. Ködderitzsch, A. Svane, L. Petit, and H. Winter, "Electronic structures of normal and inverse spinel ferrites from first principles," Phys. Rev. B **74**, 174431 (2006).

[58]A. Rogalev, J. Goulon, F. Wilhelm, Ch. Brouder, A. Yaresko, J. Ben Youssef, and M. V. Indenbom, "Element selective X-ray magnetic circular and linear dichroisms in ferrimagnetic yttrium iron garnet films," J. Magn. Magn. Mater. **321**, 3945 (2009).

[59]X. Liang, Y. Zhu, B. Peng, L. Deng, J. Xie, H. Lu, M. Wu, and L. Bi, "Influence of interface structure on magnetic proximity effect in $Pt/Y_3Fe_5O_{12}$ heterostructures," ACS Appl. Mater. Interfaces **8**, 8175 (2016).

[60]J. M. D. Coey, *Magnetism and Magnetic Materials* (Cambridge University Press, 2010).

[61]K. Uchida, R. Iguchi, S. Daimon, R. Ramos, A. Anadón, I. Lucas, P. A. Algarabel, L. Morellón, M. H. Aguirre, M. R. Ibarra, and E. Saitoh, "Enhancement of the spin Peltier effect in multilayers," Phys. Rev. B **95**, 184437 (2017).

[62]J. M. De Teresa, A. Fernández-Pacheco, L. Morellón, J. Orna, J. A. Pard, D. Serrate, P. A. Algarabel, and M. R. Ibarra, "Magnetotransport properties of

Fe_3O_4 thin films for applications in spin electronics," Microelectron. Eng. **84**, 1660 (2007).

[63]J. Orna, P. A. Algarabel, L. Morellón, J. A. Pardo, J. M. De Teresa, R. López Antón, F. Bartolomé, L. M. García, J. Bartolomé, J. C. Cezar, and A. Wildes, "Origin of the giant magnetic moment in epitaxial Fe_3O_4 thin films," Phys. Rev. B **81**, 144420 (2010).

[64]S. Tanuma, C. J. Powell, and D. R. Penn, "Calculations of electron inelastic mean free paths. IX. Data for 41 elemental solids over the 50 eV to 30 keV range," Surf. Interface Anal. **43**, 689 (2011).

[65]M. Ziese and H. J. Blythe, "Magnetoresistance of magnetite," J. Phys. Condens. Matter **12**, 13 (2000).

[66]A. Bollero, M. Ziese, R. Höhne, H. C. Semmelhack, U. Köhler, A. Setzer, and P. Esquinazi, "Influence of thickness on microstructural and magnetic properties in Fe_3O_4 thin films produced by PLD," J. Magn. Magn. Mater. **285**, 279 (2005).

[67]L. F. Mattheiss and R. E. Dietz, "Relativistic tight-binding calculation of core-valence transitions in Pt and Au," Phys. Rev. B **22**, 1663 (1980).

[68]J. Bartolomé, F. Bartolomé, L. M. García, E. Roduner, Y. Akdogan, F. Wilhelm, and A. Rogalev, "Magnetization of Pt_{13} clusters supported in a NaY zeolite: A XANES and XMCD study," Phys. Rev. B **80**, 014404 (2009).

[69]B. T. Thole, P. Carra, F. Sette, and G. van der Laan, "X-ray circular dichroism as a probe of orbital magnetization," Phys. Rev. Lett. **68**, 1943 (1992).

[70]P. Carra, B. T. Thole, M. Altarelli, and X. Wang, "X-ray circular dichroism and local magnetic fields," Phys. Rev. Lett. **70**, 694 (1993).

[71]Since the XMCD sum rules give an average value of magnetic moments in a Pt film and the proximity-induced Pt ferromagnetism is confined in the vicinity of the Pt/ferromagnet interface,[47] the m_{tot} value increases (decreases) with decreasing (increasing) Pt thickness. On the other hand, in the case of the XRMR, since the spatial profile of the Pt magnetic moment is computed in analysis processes, the derived m_{tot} value is independent of the Pt thickness.[52]

[72]G. F. Dionne, *Magnetic Oxides* (Springer, New York, 2009).

[73]P. Bougiatioti, O. Manos, O. Kuschel, J. Wollschläger, M. Tolkiehn, S. Francoual, and T. Kuschel, "Impact of magnetic moment and anisotropy of $Co_{1-x}Fe_x$ thin films on the magnetic proximity effect of Pt," e-print arXiv:1807.09032 (2018).